Neuron
Article

NMDAR-Regulated Dynamics of Layer 4 Neuronal Dendrites during Thalamocortical Reorganization in Neonates

Hidenobu Mizuno,[1,2] Wenshu Luo,[1,2] Etsuko Tarusawa,[3] Yoshikazu M. Saito,[5] Takuya Sato,[1] Yumiko Yoshimura,[3,4] Shigeyoshi Itohara,[5] and Takuji Iwasato[1,2,*]
[1]Division of Neurogenetics, National Institute of Genetics, Mishima 411-8540, Japan
[2]Department of Genetics, SOKENDAI, Mishima 411-8540, Japan
[3]Division of Developmental Neurophysiology, National Institute for Physiological Sciences, Okazaki 444-8585, Japan
[4]Department of Physiological Sciences, SOKENDAI, Okazaki 444-8585, Japan
[5]Laboratory for Behavioral Genetics, RIKEN Brain Science Institute, Wako 351-0198, Japan
*Correspondence: tiwasato@nig.ac.jp
http://dx.doi.org/10.1016/j.neuron.2014.02.026

SUMMARY

Thalamocortical (TC) connectivity is reorganized by thalamic inputs during postnatal development; however, the dynamic characteristics of TC reorganization and the underlying mechanisms remain unexplored. We addressed this question using dendritic refinement of layer 4 (L4) stellate neurons in mouse barrel cortex (barrel cells) as a model; dendritic refinement of L4 neurons is a critical component of TC reorganization through which postsynaptic L4 neurons acquire their dendritic orientation toward presynaptic TC axon termini. Simultaneous labeling of TC axons and individual barrel cell dendrites allowed in vivo time-lapse imaging of dendritic refinement in the neonatal cortex. The barrel cells reinforced the dendritic orientation toward TC axons by dynamically moving their branches. In N-methyl-D-aspartate receptor (NMDAR)-deficient barrel cells, this dendritic motility was enhanced, and the orientation bias was not reinforced. Our data suggest that L4 neurons have "fluctuating" dendrites during TC reorganization and that NMDARs cell autonomously regulate these dynamics to establish fine-tuned circuits.

INTRODUCTION

During early postnatal development, neuronal activities of thalamocortical (TC) axons that innervate layer 4 (L4) of the cortex play a critical role in the refinement of TC circuits (Hubel et al., 1977; Goodman and Shatz, 1993; Katz and Shatz, 1996; Sur and Rubenstein, 2005). L4 of the mouse somatosensory cortex (barrel cortex) has an array of "barrels" that correspond to the arrangement of whiskers on the face (Woolsey and Van der Loos, 1970; Erzurumlu and Kind, 2001; Fox, 2008). TC axon terminals from the ventral posteromedial (VPM) nucleus are clustered in the barrel center, L4 spiny stellate neurons (barrel cells) are located around the barrel edge, and dendrites of barrel cells are asymmetrically oriented toward the barrel center (Woolsey and Van der Loos, 1970; Woolsey et al., 1975; Erzurumlu and Jhaveri, 1990; Erzurumlu and Kind, 2001; Barnett et al., 2006a; Fox, 2008). These morphological features of barrels, which are related to the exquisite sensitivity of whiskers in mice (Petersen, 2007), are formed during neonatal stages under the influence of inputs from the whiskers (Woolsey and Wann, 1976; Ohsaki et al., 2002) and the thalamus (Narboux-Nême et al., 2012; Li et al., 2013). Because of these unique characteristics, barrel formation has been studied as it is an excellent model for understanding the mechanisms underlying the activity-dependent refinement of TC connectivity during postnatal life.

Mouse genetic studies have unraveled the molecular basis of the activity-dependent formation of barrel morphologies (Cases et al., 1996; Welker et al., 1996; Iwasato et al., 1997; Erzurumlu and Kind, 2001; Inan and Crair, 2007; Wu et al., 2011). Molecules that are involved in glutamate release and serotonergic regulation on the presynaptic side of TC connectivity have been suggested to play a role in barrel formation (Cases et al., 1996; Welker et al., 1996; Persico et al., 2001; Iwasato et al., 2008; Narboux-Nême et al., 2012). On the other hand, glutamate receptors and their downstream candidates have been suggested to be involved on the postsynaptic side (Iwasato et al., 2000; Hannan et al., 2001; Barnett et al., 2006b; Ince-Dunn et al., 2006; Iwasato et al., 2008; Ballester-Rosado et al., 2010). Among the many molecules that have been identified, the N-methyl-D-aspartate (NMDA)-type ionotropic glutamate receptor (NMDAR), which plays a critical role in plasticity primarily on the postsynaptic side during development and in adulthood (Cline and Constantine-Paton, 1990; Tsien et al., 1996; Sin et al., 2002; Wong and Ghosh, 2002), is a key player in barrel formation. The cortex-specific knockout (KO) of NR1, the essential subunit of NMDAR, has been shown to disrupt the morphological features of barrels, including the barrel-center clustering of TC axon terminals, the barrel-edge localization of barrel cells, and the biased orientation of barrel cell dendrites toward the barrel center, indicating the importance of cortical NMDARs in barrel formation (Iwasato et al., 2000; Datwani et al., 2002; Lee et al.,

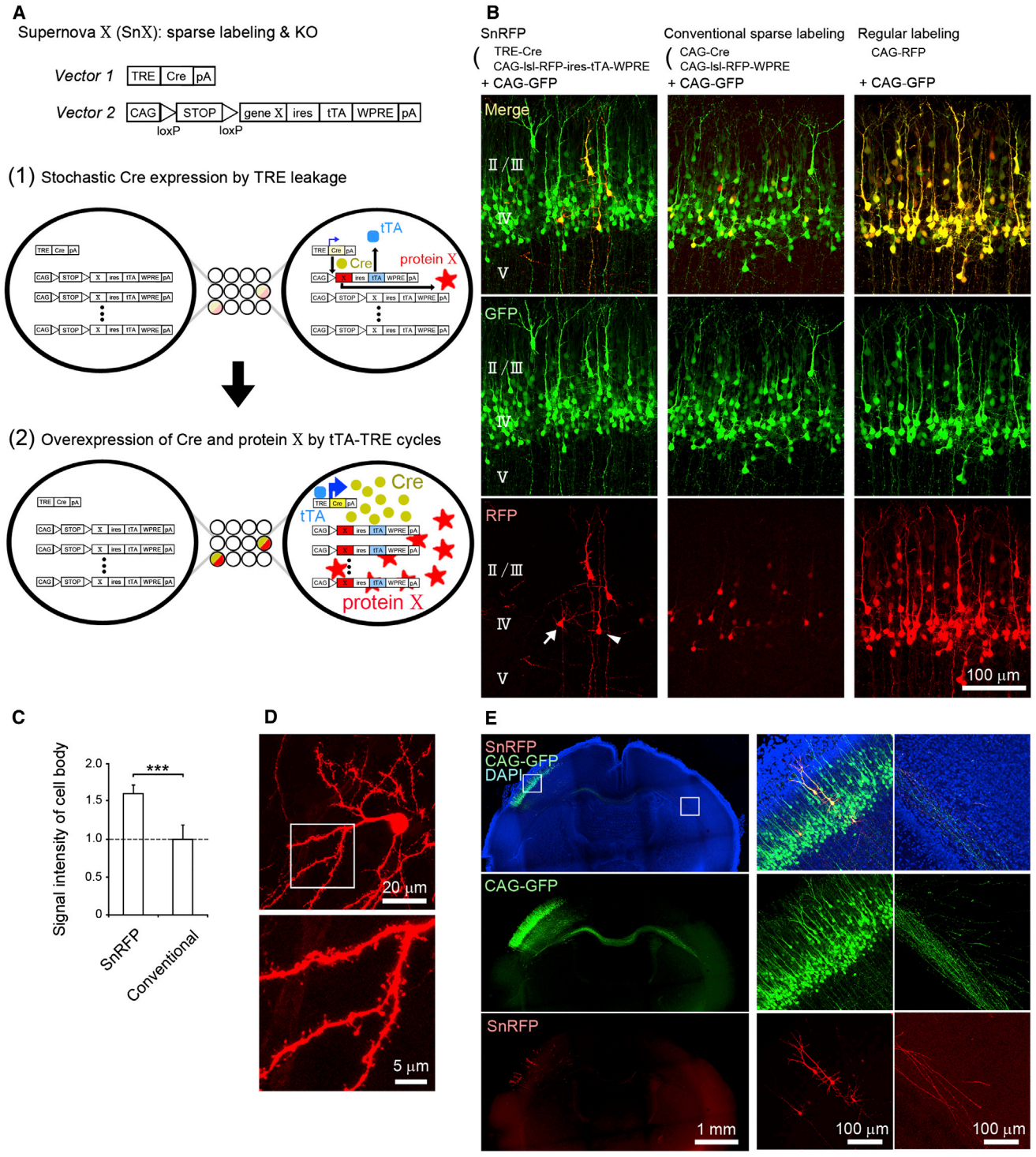

Figure 1. The Supernova System Enables Sparse and Bright Labeling of Cortical Neurons

(A) Schematic of the "Supernova" system. (1) In neurons carrying both vector 1 and vector 2, leakage from the tetracycline response element (TRE) drives weak *Cre* expression on rare occasions. Only in these sparse populations of neurons, Cre excises loxP-STOP-loxP cassette from a few copies of vector 2, and *tetracycline trans-activator* (*tTA*) is expressed from the strong CAG promoter. (2) tTA enhances *Cre* expression by binding to TRE. This positive feedback of the tTA-TRE cycles facilitates expression of Cre and "protein X" (e.g., RFP, GCaMP3) in the sparse population of transfected cells.

(B) Vectors were delivered to layer 4 (L4) excitatory neurons by in utero electroporation (IUE) at embryonic day 14 (E14), and coronal sections were made at postnatal day 4 (P4). The CAG-GFP vector was cotransfected to label the transfected neurons. The Supernova RFP (SnRFP) labeling (left) was as sparse as the

(legend continued on next page)

2005). Furthermore, a recent single-cell KO study of NR2B, the predominant NR2 subunit of NMDAR in the developing cortex, has shown that biased dendritic orientation is impaired in NR2B-lacking barrel cells, suggesting a cell-autonomous function of NMDARs in establishing the biased dendritic orientation of barrel cells (Espinosa et al., 2009).

Despite nearly half a century of research on barrels (Woolsey and Van der Loos, 1970), the dynamics of barrel formation in the neonatal cortex and the associated molecular mechanisms operating in the neonatal cortex remain unexplored. To address these issues, we focused on the dynamic role of NMDAR signaling in dendritic refinement of barrel cells and analyzed the dynamic processes in normal and NMDAR-deficient (NR1 KO) barrel cells in the neonatal cortex. For this purpose, we developed the following two systems: (1) the "Supernova" system that enabled bright labeling of single L4 neurons and labeled neuron-specific gene targeting in living neonates and (2) TC axon-green fluorescent protein (TCA-GFP) transgenic (Tg) mice that enabled us to visualize the presynaptic TC axon clusters in vivo. We then performed in vivo time-lapse imaging and detailed histological analyses of dendritic refinements in normal and NMDAR-deficient barrel cells. Our results suggested that cortical dendrites are highly motile during TC reorganization and that these dendritic "fluctuations" are regulated by cell-autonomous functions of NMDARs that are activated by thalamic inputs in both cell-wide and location-specific manners.

RESULTS

The Supernova System: A Method for Single-Cell Labeling and Labeled Cell-Specific Gene KO

To visualize the morphological changes of barrel cell dendrites in deep cortical layers in living neonates, it is essential to label neurons sparsely and extremely brightly. In order to express a gene of interest (*gene X*) in a sparse population of neurons, we developed the "Supernova X (SnX)" system consisting of tetracycline response element (TRE)-Cre (vector 1) and CAG-loxP-STOP-loxP-(gene X)-ires-tTA-WPRE (vector 2) (Figure 1A). This system was inspired by our observation that TRE occasionally drives gene expression, although extremely weakly, even in the absence of tetracycline transactivator (tTA) stimulation. In this system, leakage of TRE drives the weak expression of *Cre* and, subsequently, *tTA* in a very small population of neurons that carry both vectors. Thus, only in these cells, the expression of *gene X* is facilitated by the positive feedback of the tTA-TRE cycles.

We transfected L4 neurons by in utero electroporation (IUE) (Mizuno et al., 2007) at embryonic day (E) 14 with Supernova-red fluorescent protein (SnRFP); the transfected cells were labeled with CAG-GFP, which was cotransfected (Figure 1B). The barrel cortex L4 contains two types of excitatory neurons, spiny stellate neurons (barrel cells, the major type) and star pyramids (the minor type), which are distinguished by the absence and presence of an apical dendrite, respectively (Staiger et al., 2004; Callaway and Borrell, 2011). Both types of cells were labeled by IUE (Figure 1B, bottom left). We quantified the ratio of RFP-expressing neurons to GFP-expressing neurons at postnatal day (P) 8 and found that only 5.6% ± 0.8% (n = 5 mice) of the GFP-labeled neurons coexpressed RFP, confirming the sparseness of SnRFP labeling. Importantly, fluorescence in the majority (64.6% ± 5.6%; n = 6 mice) of the SnRFP-labeled neurons was bright enough to allow clear visualization of their dendritic morphologies (RFP^{high} neurons). SnRFP-labeled RFP^{high} neurons were so brightly labeled that spines and long axons could also be visualized (Figures 1C–1E).

To understand the cell-autonomous function of a gene such as *NR1*, a single-cell KO system is required. As shown in Figure 1A, our Supernova system was designed to achieve high levels of Cre expression only in the labeled neurons. To examine the efficiency and specificity of the Supernova system in the excision of a floxed fragment from the chromosome, we transfected CAG-loxP-CAT-loxP-GFP reporter Tg mice, which express GFP when the loxP-CAT-loxP cassette is excised by Cre-mediated recombination, with SnRFP (Figure 2A). At P8, the majority of RFP-positive cells (359/397 cells; 6 mice) and all RFP^{high} cells (291/291 cells) expressed GFP. Conversely, all GFP-labeled cells (359/359 cells) expressed RFP. These results indicate that genomic recombination was highly specific to the RFP-positive neurons. Next, we examined the efficiency of the Supernova system in deleting the floxed NR1 allele ($NR1^{f}$) from the chromosome (Tsien et al., 1996; Iwasato et al., 2000) (Figures 2B–2G). To assess the disruption of functional NMDAR in Supernova-labeled cortical neurons, we performed calcium imaging on dissociated cultures from P0 $NR1^{f/+}$ and $NR1^{f/f}$ pups that were transfected with Supernova GCaMP3 (SnGCaMP3) in L4 neurons. Addition of NMDA and glycine to the cultures increased GCaMP3 fluorescence in $NR1^{f/+}$ (control) but not in $NR1^{f/f}$ (NR1 KO) neurons, indicating efficient NR1 disruption in NR1 KO neurons (Figures 2B–2E). We further confirmed the disruption of functional NMDAR in Supernova-labeled cortical neurons by slice electrophysiology. Cortical slices were prepared from P5–P7 $NR1^{f/+}$ and $NR1^{f/f}$ pups that were transfected with SnRFP in L4 neurons by IUE, and whole-cell patch-clamp recordings were performed to compare the NMDA- and AMPA-mediated excitatory postsynaptic currents (EPSCs). RFP^{high} neurons in $NR1^{f/+}$ and $NR1^{f/f}$ mice were referred to as control and NR1

conventional sparse labeling (middle; a combination of the CAG-Cre and CAG-loxP-STOP-loxP (lsl)-RFP-WPRE [Dhande et al., 2011; Sato et al., 2012]) and as bright as regular labeling with the CAG-RFP labeling (right). Spiny stellate cell (arrow) and star pyramid (arrowhead) can be distinguished by the absence and presence of the apical dendrite, respectively (bottom left).

(C) The average brightness of cell bodies of RFP^{high} neurons labeled by the SnRFP (n = 36) was about 160% of that of RFP^{high} neurons labeled by the conventional method (n = 28; p = 0.0005). Values are represented as mean ± SEM.

(D) Dendritic spines were also clearly visible with SnRFP labeling in barrel cells at P16. Bottom: higher-magnification image of the square in the top panel.

(E) SnRFP labeling was bright enough to visualize the individual callosal axons. Left: low-power images of a coronal section through the P4 somatosensory cortex transfected with CAG-GFP and SnRFP by IUE. Middle: the transfected side: higher-magnification images of the left square in the left panel. Right: higher-magnification images of the right square in the left panel. Single callosal axons were labeled by SnRFP.

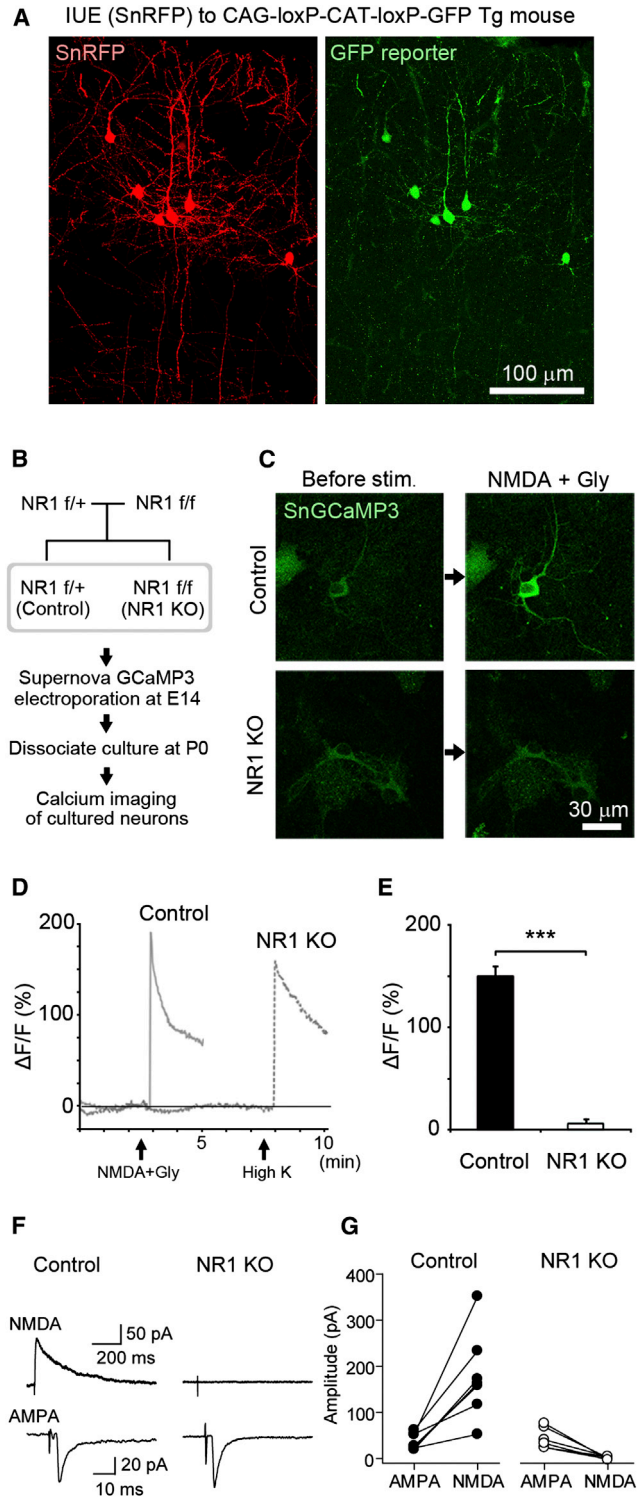

Figure 2. The Supernova System Enables Gene Knockout Only in the Sparsely Labeled Neurons

(A) Genomic recombination in a CAG-loxP-CAT-loxP-GFP Tg reporter mouse, which is indicated by the GFP signals, is specific to the SnRFP-labeled neurons. SnRFP vector set was introduced to L4 of reporter mouse by IUE and the section was cut at P8.

KO cells, respectively. We observed NMDAR-mediated currents in control but not in NR1 KO cells (Figures 2F and 2G). Taken together, these data indicate that the Supernova system was highly effective for sparse and bright cell labeling with a low background and for labeled cell-specific gene targeting.

TCA-GFP Mouse: A Tg Mouse Line for Barrel Map In Vivo Labeling

To observe the barrel map in vivo, fluorescent-labeled TC axons are indispensable. We generated Tg mouse lines (TCA-GFP) that expressed the membrane-bound enhanced GFP from the sensory thalamus-specific serotonin transporter (5-HTT) promoter (Figure 3A). From ten Tg founder mice, we selected the line (40) with the brightest GFP expression that was highly restricted to the somatosensory, visual, and auditory thalamic subdivisions during early postnatal development (Figures 3B, 3C, and S1 available online). We were able to observe the barrel map in this line without sectioning (Figure 3B). The time course of barrel map formation was characterized in tangential cortical slices from TCA-GFP mice. Barrel rows began to segregate at approximately P2, followed by segregation of individual barrel patches at approximately P3. The barrel edges were obvious at approximately P4 (Figure 3D). The IUE-mediated transfection of SnRFP into TCA-GFP mice enabled simultaneous RFP and GFP labeling of single barrel cells and the barrel map, respectively (Figure 3E and Movie S1).

Cell-Autonomous Roles of Neonatal NMDAR in Dendritic Refinement of Barrel Cells

We first examined whether the Supernova-mediated single-cell KO of NR1 impairs the dendritic refinement of barrel cells in a cell-autonomous manner by confocal analysis of brain slices prepared at P16 (after the maturation of barrel cells) (Figures 4A–4H and Figures S2A–S2D). SnRFP was introduced into the L4 neurons by IUE into E14 embryos from an intercross between TCA-GFP;NR1$^{f/+}$ males and NR1$^{f/f}$ females (Figure 4A), and only TCA-GFP-labeled pups, in which the ratio of NR1$^{f/+}$ and NR1$^{f/f}$ pups was 1:1, were used for further analyses. The RFP^{high} neurons without apical dendrites were identified as barrel cells, and barrel cells located around the barrel edge that was defined by GFP signals were used for analyses (Figure 4B). The genotypes of the pups were revealed only after analyses, and the RFP^{high} neurons in TCA-GFP;NR1$^{f/+}$ and TCA-GFP;NR1$^{f/f}$ mice were referred to as control and NR1 KO cells, respectively. The

(B) Experimental protocol for in vitro calcium imaging.
(C) Example images of in vitro calcium imaging. NMDA and glycine were added to obtain an NMDAR-mediated response.
(D) Representative traces. Because NR1 KO cells failed to respond to NMDA+gly application, calcium responsiveness of GCaMP3 of these cells was confirmed with 30 mM KCl (high K).
(E) Addition of NMDA and glycine increased GCaMP3 fluorescence in NR1$^{f/+}$ (control: n = 11) but not in NR1$^{f/f}$ (NR1 KO: n = 10; $p < 0.00001$) neurons. Values are represented as mean ± SEM.
(F) Comparison of NMDA- and AMPA-mediated EPSCs. Representative NMDA- (top) and AMPA- (bottom) EPSCs (average of ten sweeps) were shown for control (left) and NR1 KO (right) cells.
(G) Average amplitude of AMPA and NMDA EPSCs. Number of cells: 7 (control: left) and 7 (NR1 KO: right).

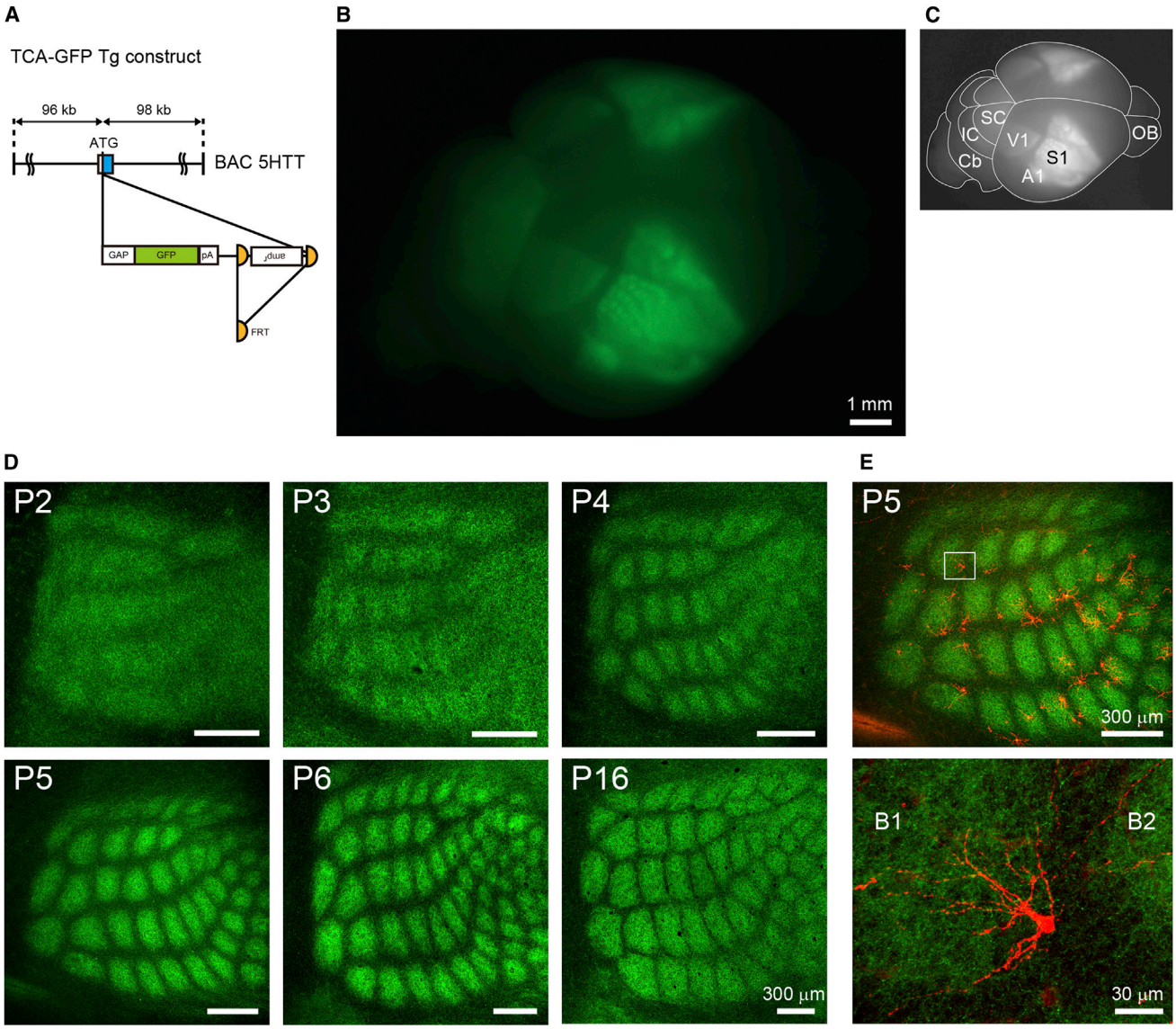

Figure 3. Generation of TCA-GFP Mice with a High Level of GFP Expression in Thalamocortical Axons

(A) The translational initiation site of the *serotonin transporter* (*5HTT*) gene on a bacterial artificial chromosome (BAC) clone was replaced with the coding sequence of membrane-bound enhanced GFP, and the Amp selection marker was subsequently removed by flp/FRT recombination in bacteria. This BAC construct was microinjected into fertilized eggs to generate TCA-GFP mice.

(B and C) Barrel maps are visible in a whole-brain preparation from TCA-GFP mice at P7. Brain areas are shown in (C). S1, primary somatosensory cortex; V1, primary visual cortex; A1, primary auditory cortex; OB, olfactory blub; SC, superior colliculus; IC, inferior colliculus; Cb, cerebellum.

(D) Confocal images of tangential sections showing the maturation of the GFP-labeled barrel map in TCA-GFP mice.

(E) Simultaneous labeling of the barrel map and individual L4 excitatory neurons at P5. Bottom panel shows higher magnification image of the square region in the top panel. A typical SnRFP-labeled barrel cell is shown.

See also Figure S1 and Movie S1.

average dendritic length of NR1 KO cells did not differ from that of control cells (Figure 4C). However, in NR1 KO cells, the dendritic length inside the barrel was smaller, and the dendritic length outside the barrel was larger, than in control cells (Figures 4D and 4E). Consequently, the orientation bias index (OBI) toward the barrel center, defined as the ratio of the inside length to the total length, was significantly lower in NR1 KO cells than that in control cells (Figure 4F). The density of spines inside barrels was also significantly lower in NR1 KO barrel cells than that in control cells (Figures 4G and 4H). These results revealed that NMDARs autonomously regulate dendritic and spine refinement in barrel cells in accordance with the results obtained from a previous single-cell NR2B KO study (Espinosa et al., 2009).

Next, we characterized the detailed developmental processes of NMDAR-dependent dendritic refinement of barrel cells in cortical slices from neonatal mice (Figures 4I–4O and Figures

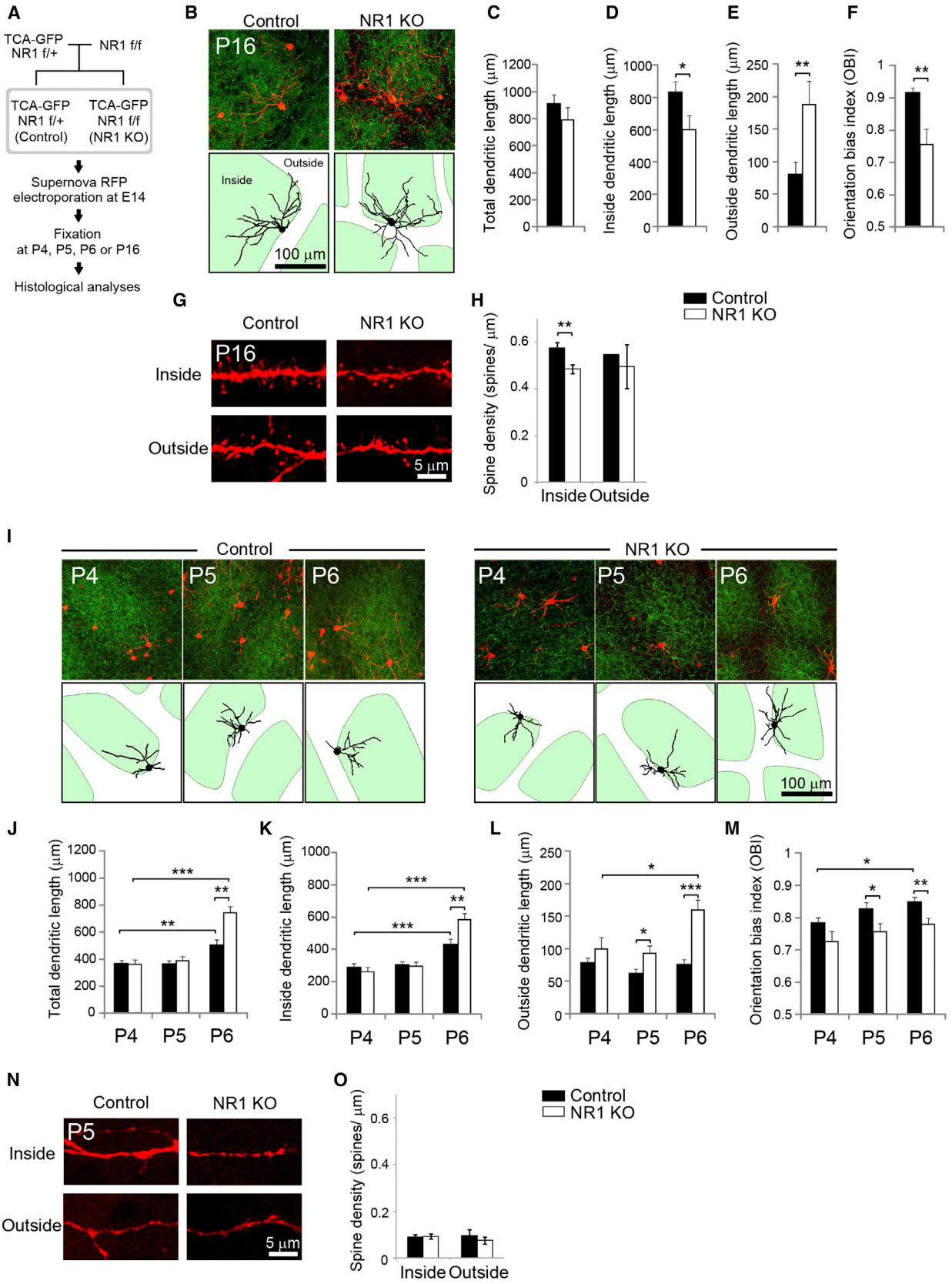

(legend on next page)

S2E–S2H). The youngest age we used was P4 because at P3, a cell-dense "barrel wall" was not visible (Figure S2I), although TC axon clusters had already started to form (Figure 3D). Furthermore, it was difficult to distinguish barrel cells from star pyramids because their morphologies are similar at P3 (H.M. and T.I., unpublished data; see also Callaway and Borrell, 2011). At P4, there were no differences in the inside, outside, and total dendritic lengths and OBIs between NR1 KO and control cells (Figures 4J–4M). In control cells, the inside dendritic length at P6 was larger than that at P4 and the outside dendritic length at P6 and P4 were similar, thus OBI at P6 was larger than that at P4 (Figures 4K–4M). In contrast, in NR1 KO cells, both inside and outside dendritic lengths at P6 were larger than those at P4, and OBIs at P6 and P4 were similar (Figures 4K–4M). As a consequence, OBIs were significantly larger in control cells at P5 and P6 than those in NR1 KO cells (Figure 4M). These results revealed that the NMDAR cell autonomously regulates dendritic refinement of barrel cells during the early postnatal period between P4 and P6.

In Vivo Time-Lapse Imaging of Dendritic Refinement of Barrel Cells in Neonates

We used TCA-GFP pups in which L4 neurons were labeled with SnRFP-IUE and made a cranial window over the large barrels (arcs 1–5) identified by GFP fluorescence (Figures 5A and 5B). Then, using a two-photon microscope (Svoboda et al., 1997), we simultaneously observed GFP-labeled barrel patches and SnRFP-labeled barrel cells in vivo (Figure 5C). GFP-labeled TC axon clusters were used to easily identify L4 neurons (Figures 5C and 5D) that were otherwise difficult to recognize in the living neonatal cortex because the cortical thickness markedly changes during early postnatal development and the layer specificity of IUE-mediated labeling is not perfect.

We performed time-lapse imaging of the morphological changes that occurred in normal (control) barrel cells over a period of 9 hr starting at P4 and 18 hr starting at P5 (Figures 5E and 6A–6F, Figure S3, and Movies S2 and S3; see also Supplemental Experimental Procedures). Histological analyses were performed in some experiments immediately after imaging in order to verify the accuracy of the in vivo imaging results (Figures 5F and 5G). We primarily analyzed the results obtained after 18-hr-long imaging sessions that started at P5, because at this age, we were able to perform longer imaging than that at P4. We measured the dendritic lengths inside and outside the barrel of each P5 cell at 0, 9, and 18 hr after the first imaging session and analyzed the changes in OBIs of dendritic length. OBI of control cells (n = 4) significantly increased over 18 hr (Figure 6C). Next, we examined dendritic extension and retraction (represented as positive and negative values, respectively) of each branch length of the control cells over 18 hr and found that extensions in the branch lengths inside the barrel were significantly larger than those outside the barrel (Figure 6D). These results were consistent with our histological results of newborn pups maintained under normal conditions (Figures 4K–4M), suggesting that dendritic refinement occurred normally under our imaging conditions. Thus, the 18-hr-long imaging session initiated at P5 was useful for analyzing the refinement of barrel cell dendrites in vivo.

Comparisons of the images at 0 and 18 hr in P5 control cells showed that branch elongation and retraction occurred both inside and outside the barrels (Figures 6B and 6E and Movie S4), indicating that the dendritic branches were highly dynamic in the neonatal cortex. To further confirm the dynamic branch movements, we compared the morphologies of each branch in control cells at 0, 9, and 18 hr. Branch behaviors during each 9 hr period were categorized as stabilized (S: length changes within ±3 μm), elongated (E: elongated more than 3 μm), and retracted (R: retracted more than 3 μm). Branch behaviors during the 18 hr period were categorized into the following 9 types: EE, ER, ES, RE, RR, RS, SE, SR, and SS (Figures S3B and S3C). Approximately half of the inner (48%) and outer (56%) branches in the control cells were ER or RE (Figure 6F), indicating that branch tip behavior easily shifted between elongation and retraction or vice versa. These results clearly showed the dynamic and concurrent elongation and retraction of branch tips during dendritic refinement in normal neonatal barrel cells.

In Vivo Time-Lapse Imaging of Dendritic Refinement of NMDAR-Deficient Barrel Cells

Finally, we analyzed the dendritic dynamics in NR1 KO barrel cells (Figures 6G–6L). In NR1 KO cells (n = 8), OBI did not change

Figure 4. Histological Analyses of Dendritic Refinement of Barrel Cells in Neonates

(A) Experimental protocol for histological analyses of barrel cell dendrites.

(B) Representative images (top) and traces (bottom) of barrel cell dendrites at P16. Barrel borders were identified using TCA-GFP fluorescence (see Supplemental Experimental Procedures).

(C–F) Quantification of dendritic morphologies of mature (P16) barrel cells. The entire dendritic length of NR1 KO cells (n = 11) was similar to that of control cells (C; n = 16, p = 0.32), but the dendritic lengths inside and outside the barrel were smaller (D; p = 0.041) and larger (E; p = 0.007), respectively, than those in control cells. The orientation bias index (OBI) toward the barrel center, which is defined as the ratio of inner dendrite length to total dendrite length, was significantly lower in NR1 KO than in control cells (F; p = 0.007).

(G and H) Representative images (G) and quantification (H) of spine density on the second dendritic segment at P16. The density of spines inside the barrel was lower in NR1 KO cells than in control cells (p = 0.005). Number of branches: inside control, 32; inside NR1 KO, 23; outside control, 1; outside NR1 KO, 6.

(I) Representative images and traces of barrel cell dendrites at P4–P6.

(J–M) Quantification of dendritic morphologies of developing barrel cells at P4–P6 (J, total length; K, inside length; L, outside length; M, OBI). At P4, OBI was similar between NR1 KO (n = 12) and control cells (M) (n = 27; p = 0.091). Although OBI gradually increased from P4 to P6 in control cells (P4 versus P6, p = 0.015, one-way ANOVA followed by Tukey test), it did not change in NR1 KO cells (P4 versus P6, p = 0.257, one-way ANOVA followed by Tukey test). At P5 and P6, OBI in NR1 KO cells (P5: n = 17; P6: n = 26) was significantly lower than that in control cells (P5: n = 17, p = 0.032; P6: n = 20, p = 0.007).

(N and O) Representative images (N) and quantification (O) of spine density on the second dendritic segment at P5. Spine densities inside and outside barrels did not differ significantly between control and NR1 KO barrel cells. Number of branches: inside control, 17; inside NR1 KO, 19; outside control, 5; outside NR1 KO, 6.

Values are represented as mean ± SEM. *p < 0.05, **p < 0.01, and ***p < 0.001.

See also Figure S2.

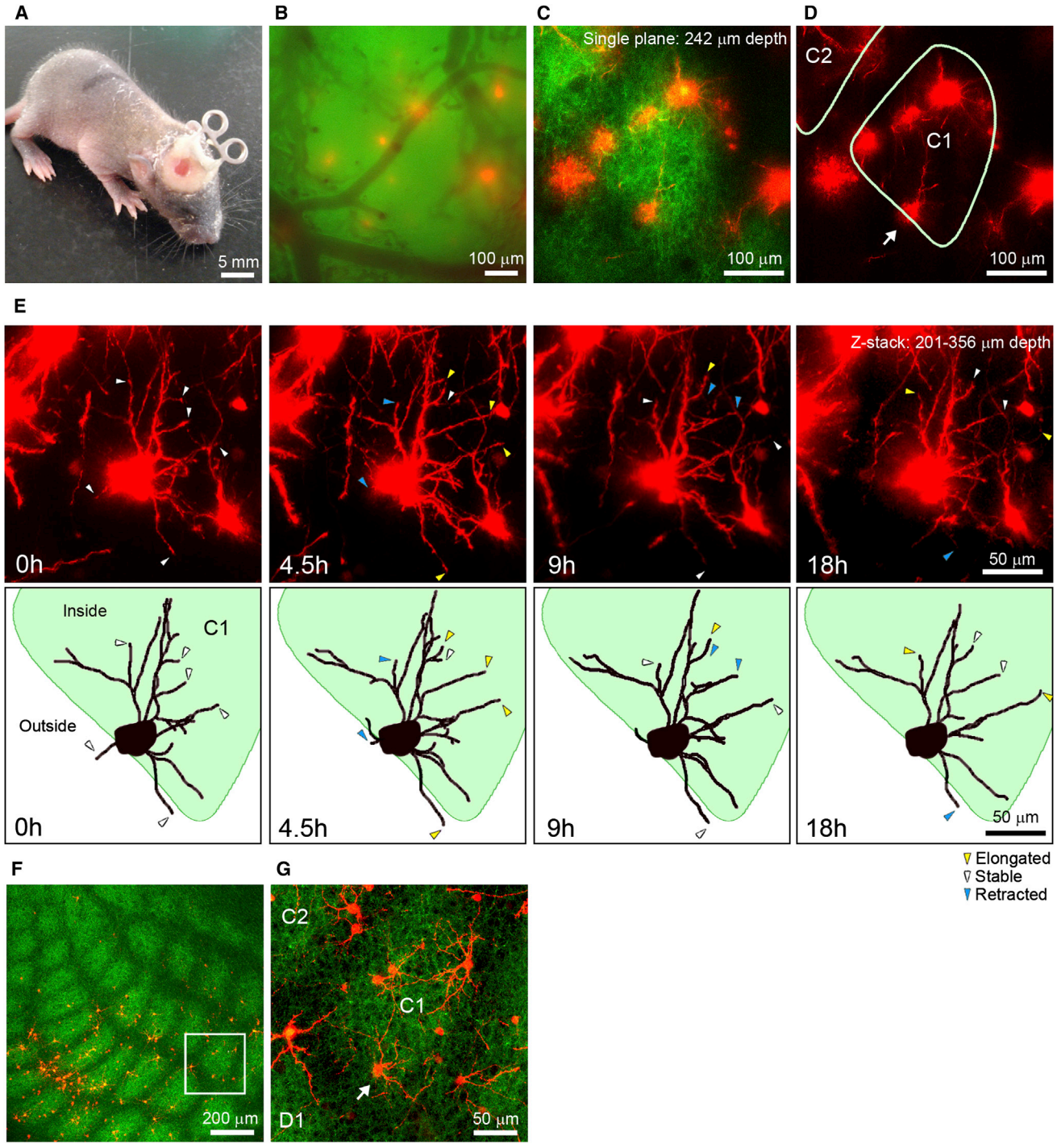

Figure 5. In Vivo Two-Photon Time-Lapse Imaging of Barrel Cell Dendrites in Neonates

(A) A small cranial window (500 μm diameter) was made on the somatosensory cortex of a P4 mouse. A custom-made titanium bar was used to fix the mouse head during the two-photon imaging.

(B) Fluorescence CCD image of the cortical surface at P5 through the cranial window.

(C and D) Two-photon images of SnRFP-labeled barrel cells in a P5 TCA-GFP mouse. Barrel edges were characterized by TCA-GFP labeling (D).

(E) Higher-magnification images (top) and traces (bottom) of a barrel cell in (D) (arrow) indicating morphological changes during the 18-hr-long imaging. Arrowheads: dendritic tips (yellow, elongated; white, stable; blue, retracted).

(F) Confocal image of tangential section made after time-lapse imaging (C–E).

(G) Higher-magnification image of the square region in (F). Same area in the two-photon image is shown in (C) and (D). Arrow indicates the same neuron in (D). See also Movies S2, S3, and S4.

significantly over 18 hr at P5 (Figure 6I). In addition, extensions in each dendritic branch inside and outside the barrel over 18 hr were not significantly different from each other (Figure 6J). These results were consistent with those of our histological analysis of newborn mice (Figures 4K–4M). Compared with the control cells (Figure 6E), NR1 KO cells showed much larger changes in the dendritic length over 18 hr (Figure 6K). The absolute values of changes of dendrite length were significantly larger in NR1 KO cells than those in control cells (Figure 6M). In contrast, the frequencies of ER or RE branch behaviors were similar in NR1 KO and control cells (Figures 6F and 6L). In summary, these results indicate that NMDAR cell autonomously and negatively regulates branch dynamics to establish the characteristic asymmetry and orientation of barrel cell dendrites.

DISCUSSION

Neuronal circuits in the mammalian cortex are refined by sensory inputs from the thalamus during early postnatal development (Hubel et al., 1977; Goodman and Shatz, 1993; Katz and Shatz, 1996; Sur and Rubenstein, 2005). Since the discovery of barrels (Woolsey and Van der Loos, 1970), the formation of their characteristic morphological features has been a central model for the developmental refinement of cortical circuits (Erzurumlu and Kind, 2001; Wu et al., 2011). In particular, dendritic refinement of barrel cells is an excellent model in which circuit reorganization in neonatal L4 induced by thalamic inputs can be quantitatively analyzed as changes in the orientation of barrel cell dendrites (Datwani et al., 2002). Our Supernova (Figures 1 and 2) and TC axon labeling (Figure 3) systems enabled us to precisely study the dynamics of neonatal barrel cell dendrites in vivo (imaging) and in vitro (histological analyses). We found the following results. First, in the neonatal cortex (between P4 and P6), barrel cell dendrites were refined by cell-autonomous NMDAR function, which increased their orientation bias toward TC axons at the barrel center (Figures 4M, 6C, and 6I). Second, NMDAR-dependent dendritic refinement involved preferential extension of the dendritic branches within the barrel (Figures 4K, 4L, 6D, and 6J). Third, individual dendritic branches inside and outside the barrel were highly motile (Figures 6A–6F). Fourth, dendritic motility was accelerated in the absence of cell-autonomous NMDAR signaling (Figures 6G–6M).

The "Dynamic Model" of Dendritic Refinement

Previous histological analyses of mature barrels have led to the conventional "steady growth model" of dendritic refinement; this model proposes that orientation is acquired by simple and steady elongation and/or elaboration inside the barrel and retraction and/or pruning outside the barrel, which occurs in an NMDAR-dependent manner (Greenough and Chang, 1988; Datwani et al., 2002; Barnett et al., 2006a; Espinosa et al., 2009) (Figure 7A). However, our in vivo imaging and detailed histological analyses in neonates support a new "dynamic model" of dendritic refinement (Figure 7B). In the wild-type barrel cells, the dendritic branches both inside and outside the barrels are motile (red and blue arrows in the wild-type in Figure 7B; Figures 5E, 6A, 6B, 6E, and 6F), possibly in search for their correct synaptic partners. Similar dendritic motility has been described in other systems such as *Xenopus* tadpoles (Sin et al., 2002) and developing zebrafish (Niell et al., 2004). Significantly increased dendritic motility in both inner and outer dendrites of NR1 KO barrel cells (demonstrated by the lengths of the red and blue arrows in Figure 7B; Figure 6M) suggests that postsynaptic NMDAR signaling suppressed the dendritic motility to a certain extent throughout the cell. These results suggest that NMDAR signals originating from inner dendrites have cell-wide effects on dendritic motility because it is likely that only inner dendrites receive inputs from the thalamus during the neonatal period. Most outer dendrites extend to the interbarrel areas (Figure 4I) where there are few if any thalamic (Bureau et al., 2006) and cortical inputs (e.g., from layer 2/3 pyramidal neurons: see P5 in Figures S4A–S4C and their legends), although we cannot exclude the possibility that there are currently unidentified inputs to the interbarrel areas in neonates. In addition, postsynaptic NMDARs inhibited the outgrowth of outer dendrites (Figure 7B; Figures 4L, 6D, and 6J), further supporting the cell-wide effect of NMDAR signaling. In parallel with the cell-wide effect, postsynaptic NMDARs may also have local effects; in wild-type cells, only the inner dendrites, which can receive synchronized inputs from the principal whisker through the VPM thalamus, were elongated (Figure 7B; Figures 4K and 6D). The local effects of NMDAR may stabilize the dendritic branches receiving synchronized thalamic inputs in order to promote their steady elongation and/or to locally cancel the dendritic outgrowth inhibition induced by the cell-wide NMDAR effects.

What are possible mechanisms that underlie the cell-wide and local effects of cell-autonomous NMDAR function on dendritic refinement of barrel cells? Cell-wide effects of NMDAR signaling may involve transcriptional regulation by calcium-dependent transcription factors such as CREB, CREST, and NeuroD2 (Konur and Ghosh, 2005; Ince-Dunn et al., 2006). The local effects of cell-autonomous NMDAR function may involve regulation of local actin cytoskeleton dynamics through activation and inactivation of Rho family GTPases by guanine nucleotide exchange factors such as Kalirin-7 and GTPase-activating proteins, including α-chimaerin (α-chimerin) (Sin et al., 2002; Van de Ven et al., 2005; Iwasato et al., 2007; Xie et al., 2007; Saneyoshi et al., 2008). In addition, the activity-dependent transcription factor BTBD3 is a strong candidate downstream mediator of the local effects of NMDAR signaling on dendritic refinement (Matsui et al., 2013). Moreover, Hebbian-type synaptic plasticity is an attractive candidate for dendritic refinement (Crair and Malenka, 1995); however, our electrophysiological analyses of neonatal cortical slices showed that the average amplitude and frequency of spontaneous EPSCs (sEPSCs) and miniature EPSCs (mEPSCs) were similar between control and NR1 KO cells, although presynaptic sources could not be identified (Figures S4D–S4F). In addition, histological analyses showed that spine densities inside and outside barrels did not differ significantly between control and NR1 KO barrel cells at P5 (Figures 4N and 4O). To understand the physiological mechanisms underlying NMDAR-dependent dendritic refinement, it would be useful to monitor calcium dynamics within barrel cell dendrites in vivo. Our Supernova system enables us to express genetically coded calcium indicators such as GCaMP6 (Chen et al., 2013) in single barrel cells (our preliminary results). By

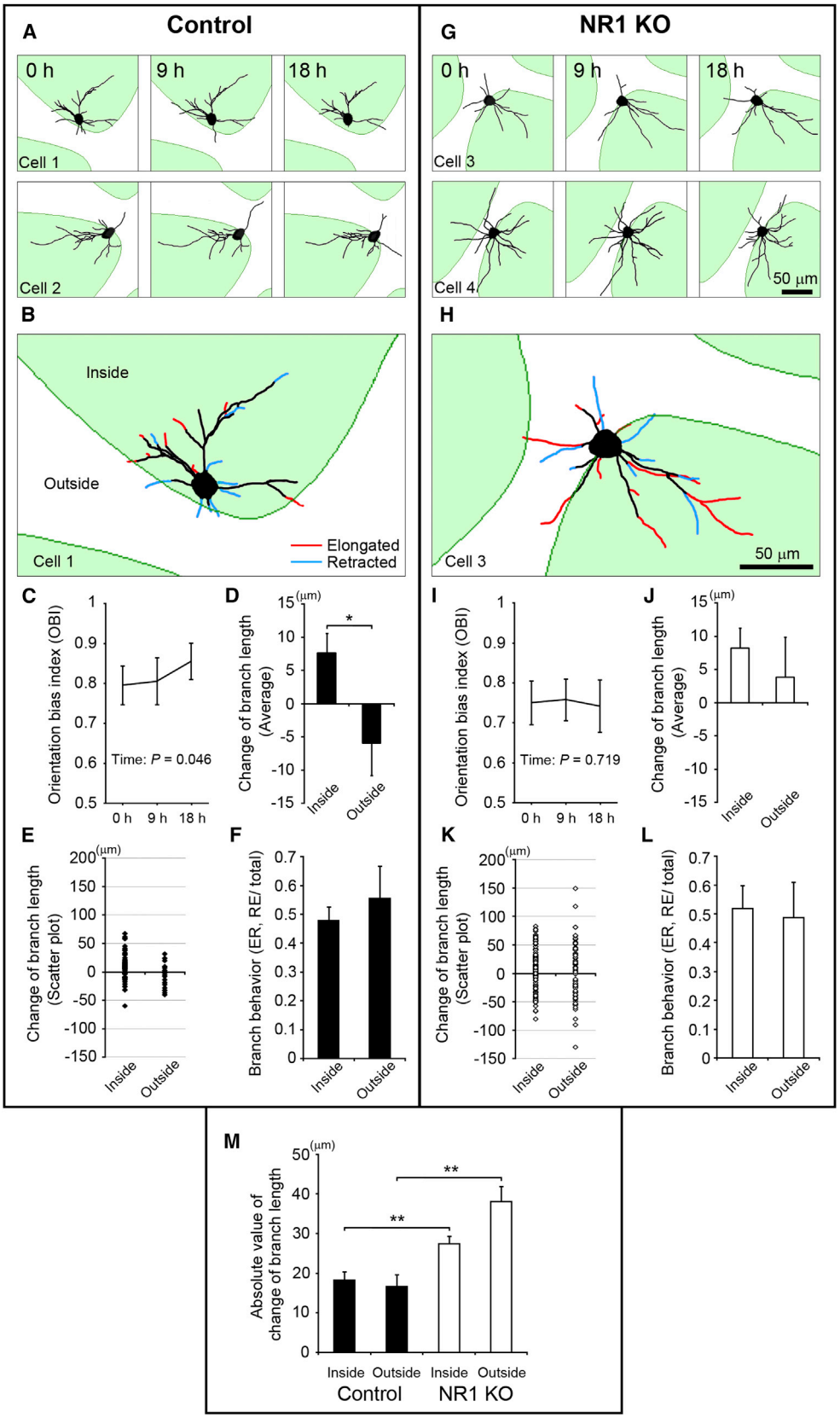

(legend on next page)

combining targeted GCaMP6 expression with long-term in vivo imaging, it will be possible to correlate calcium dynamics in individual dendritic branches with subsequent morphological changes in both control and NR1 KO barrel cells.

Cell-Autonomous and Non-Cell-Autonomous Roles of NMDAR in Barrel Cell Maturation

Histological analyses revealed some important features of dendritic refinement. At later stages of postnatal dendritic development (P16), the phenotypes of single-cell NR1 KO barrel cells described in this study, including decreased dendritic orientation bias and spine densities (Figures 4B–4H), were similar to those observed in a previous single-cell NR2B KO study (Espinosa et al., 2009), suggesting cell-autonomous NMDAR function. In contrast, some of the phenotypes shared by NR1 KO and NR2B KO barrel cells, which include normal total dendritic length, are distinct from barrel cells in cortex-specific NR1 KO mice, which lack NMDARs in all cortical excitatory neurons and some populations of glia (Iwasato et al., 2000) and exhibited larger total dendritic length and spine density compared to wild-type mice (Datwani et al., 2002). These phenotypic discrepancies between cortex-wide KO and single cortical cell KO suggest a non-cell-autonomous function of cortical NMDARs in the maturation of barrel cell dendrites and spines. NMDAR signaling in cortical excitatory neurons and/or glia may affect dendrites and spines of barrel cells through synaptic (Lefort et al., 2009) and/or gap-junction-mediated interactions (Li et al., 2012). At P4, OBIs of control and NR1 KO barrel cells were >0.5 (Figure 4M), indicating a certain degree of orientation bias toward the barrel center even at this very early stage. A similar biased orientation has been reported in normal and single-cell NR2B KO barrel cells, albeit at P6 (late neonatal stage) (Espinosa et al., 2009). The initial orientation bias at P4 could be formed by the non-cell-autonomous effects of cortical NMDAR and/or NMDAR-independent mechanisms. As a possible NMDAR-independent mechanism, barrel cell dendrites may be attracted by some unidentified guidance molecules that are possibly secreted by the TC axon terminals clustered at the barrel center (Figure 3E). Thus, barrel cell dendrites are refined during postnatal development by cooperative effects of cell-autonomous NMDAR signaling and either or both of non-cell-autonomous NMDAR signaling and NMDAR-independent mechanisms.

In Vivo Imaging of the Refinement of TC Connectivity in the Neonatal Cortex

As a first step in the in vivo imaging of the refinement in TC connectivity, we took advantage of the unique morphological features of the barrel cortex and focused on the dendritic refinement of barrel cells. In vivo imaging approaches will also be extremely useful in future studies related to barrel morphogenesis, such as the in vivo elucidation of the mechanisms that control barrel wall formation. Because barrel walls start to emerge between P3 and P4 (Figure S2I), in vivo imaging that starts at P3 or earlier should be useful to reveal how barrel walls are formed. In addition, in vivo time-lapse imaging that starts at P3 will also identify how L4 spiny stellate neurons (i.e., barrel cells) and star pyramids are differentiated because these two types of cells can be distinguished only at P4 (based on our observations and those of Callaway and Borrell, 2011). Longer-term (i.e., over a few days), shorter-interval, and/or higher-resolution (e.g., dendritic spine level) imaging will also be informative. Moreover, in vivo time-lapse imaging of KO or knockdown phenotypes of barrel-related genes (Erzurumlu and Kind, 2001; Inan and Crair, 2007; Wu et al., 2011) will yield important insights into the molecular mechanisms underlying barrel morphogenesis that cannot be obtained only by histological and physiological analyses of brain slices.

In addition to morphological studies, two-photon microscopic analyses (Carrillo et al., 2013) are also suitable for monitoring and manipulating the patterns of neuronal network activity during barrel formation at a cellular resolution by using calcium sensors such as GCaMP (Nakai et al., 2001) and optogenetic tools (Boyden et al., 2005), as partly described above. This powerful combination of morphological and functional approaches may reveal the relationship between barrel cell morphogenesis and network maturation during the critical period of barrel formation. Thus, our in vivo imaging studies of one aspect of the cell-autonomous role of NMDAR in barrel formation is a key starting point for further investigation of mechanisms underlying the activity-dependent refinement of cortical circuits in neonates.

The Supernova System: A General Method for Single-Neuron Labeling and Gene KO

The development of tools for single-neuron labeling and labeled neuron-specific gene KO in mice would facilitate understanding of the molecular and cellular mechanisms of neuronal circuit development and function. For this purpose, genetics-based

Figure 6. Barrel Cell Dendrites Show Highly Dynamic Elongation and Retraction, and NMDAR Stabilizes Dendritic Branches and Enhances Orientation Preference

(A and G) Example traces showing morphological changes of control (A) and NR1 KO (G) barrel cell dendrites over 18 hr at P5.

(B and H) Representative changes of dendritic morphologies between 0 hr and 18 hr at P5.

(C and I) OBI of dendritic length changes over 18 hr at P5. OBI was increased significantly in control cells ($p = 0.046$, repeated-measures ANOVA) (C); OBI was not changed in NR1 KO cells ($p = 0.719$, repeated-measures ANOVA) (I).

(D, E, J, and K) Quantitative analyses of morphological changes of barrel cell dendrites over 18 hr (between 0 hr and 18 hr) at P5. Barrel inside-preferred extension of dendritic branches was observed in control cells (D; inside: n = 63 branches; outside: n = 18 branches; 4 cells from 2 animals; $p = 0.030$) but not in NR1 KO cells (J; inside: n = 131 branches; outside: n = 65 branches, 8 cells from 4 animals; $p = 0.51$). Scatter plots of change of each branch length of control and NR1 KO cells were shown in (E) and (K), respectively.

(F and L) Analysis of branch behavior over 18 hr. Approximately half of the inner and outer branches in control (F) and NR1 KO (L) cells were ER or RE, indicating that branch tip behavior easily shifted between elongation (E) and retraction (R) or vice versa.

(M) Average absolute values of change of each branch length over 18 hr (between 0 hr and 18 hr; control inside versus NR1 KO inside, $p = 0.008$, Mann-Whitney U test; control outside versus NR1 KO outside, $p = 0.003$, Mann-Whitney U test). Values are represented as mean ± SEM. *$p < 0.05$ and **$p < 0.01$.

See also Figure S3.

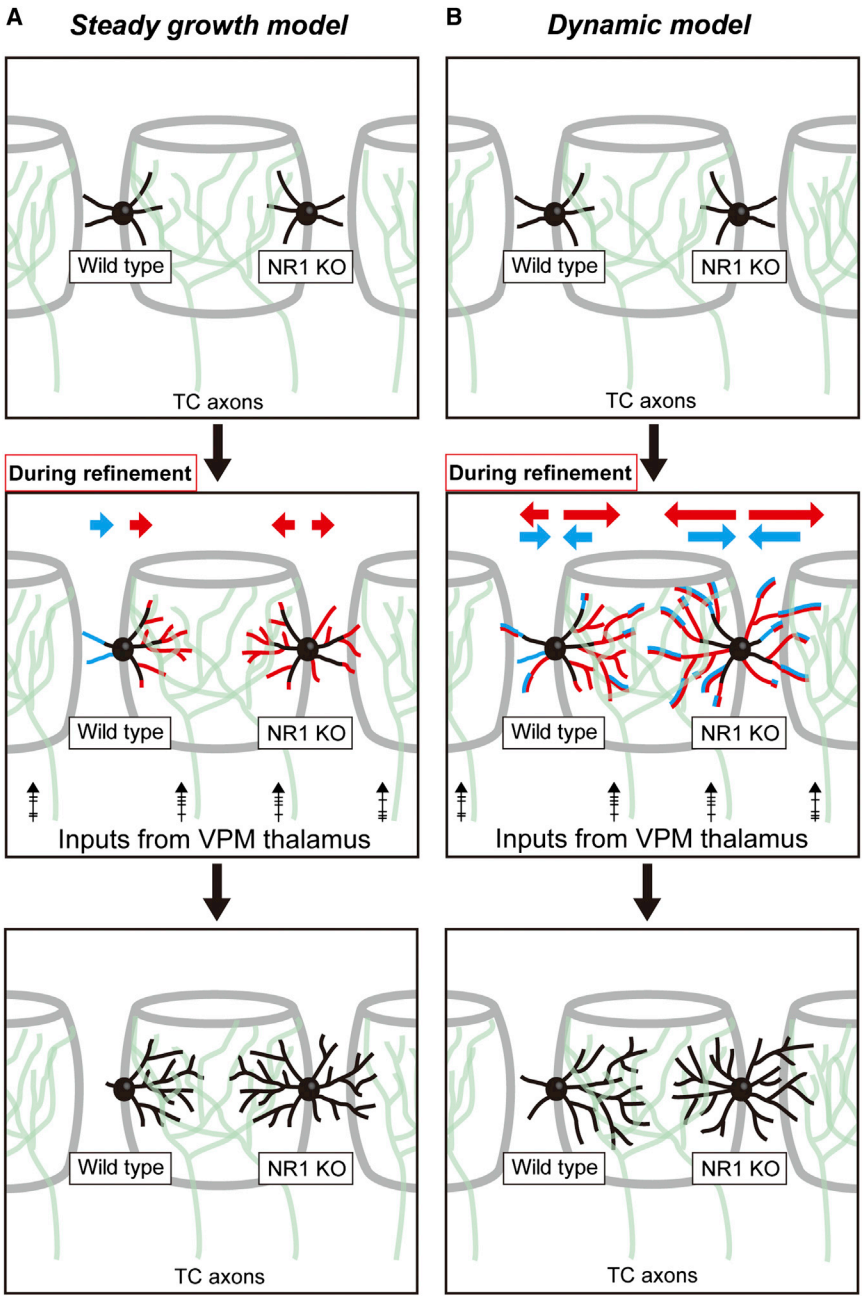

Figure 7. Models of NMDAR-Regulated Barrel Cell Dendritic Refinement in Neonatal Cortex

(A) In the conventional "steady growth model," barrel cells acquire their biased dendritic orientation by simple and steady elongation/elaboration inside (red) and retraction/pruning outside (blue) in an NMDAR-dependent manner. Therefore, dendritic length increases inside the barrel and decreases outside in wild-type cells.

(B) In the "dynamic model," both inner and outer dendrites of wild-type barrel cells are dynamic (red and blue arrows in wild-type); however, inner and outer dendrites of NR1 KO barrel cells exhibit greater motility (red and blue arrows in NR1 KO) than wild-type barrel cells. Outer dendrites are elaborated in NR1 KO barrel cells (red arrow is longer than blue arrow) but unchanged in wild-type barrel cells (red and blue arrows have the same size); inner dendrites are elaborated both in wild-type and NR1 KO barrel cells. Therefore, orientation bias toward the barrel center is formed in wild-type but not in NR1 KO barrel cells.

See text for details. See also Figure S4.

systems (e.g., the MADM and SLICK systems) have been used (Zong et al., 2005; Young et al., 2008). In order to label neurons in the developing cortex, hippocampus, and so on, IUE-based methods are also widely used (Saito and Nakatsuji, 2001; Tabata and Nakajima, 2001; Mizuno et al., 2007) and have many advantages over genetics-based methods in terms of speed, cost, required mouse space, layer specificity, and brightness. Furthermore, and more importantly, IUE-based methods make experimental design much more flexible than genetics-based methods: one can easily choose the best genetically engineered proteins (e.g., different colors of fluorescent proteins and novel calcium-sensors and optogenetic tools) for the specific purposes, from a wide variety of candidates. However, despite these many advantages of IUE-based methods, they are not suitable for single-cell labeling because they usually label neurons densely (Figure 1B, right). Although the simple combination of IUE with Cre/loxP recombination can achieve some levels of sparseness, it suffers from problems such as low intensity and high background (e.g., Figure 1B, middle).

The Supernova system described in this paper has solved these problems of IUE-based methods and achieved sparseness, brightness, and a low background of neuron labeling (Figures 1B, left, and 1C–1E). It was also suitable for gene KO specific to sparsely labeled neurons (Figure 2). Taken together, the Supernova system is a general method to express various types of proteins (such as GFP, RFP, and GCaMP) in a sparse population of neurons and can simultaneously disrupt a gene specifically in the labeled neurons; thus, the Supernova system is a promising tool to elucidate the molecular and cellular mechanisms of neuronal circuit development and function at a single-cell level.

In the current study, we conducted in vivo time-lapse imaging of the neonatal mouse cortex and analyzed both normal and impaired barrel circuit refinement. Our approach has revealed that L4 neuron dendrites are highly motile during TC circuit reorganization and this motility is autonomously regulated by cortical NMDARs.

EXPERIMENTAL PROCEDURES

Animals

All experiments were performed according to the guidelines for animal experimentation of the National Institute of Genetics (NIG). TCA-GFP mice were generated at the RIKEN Brain Science Institute (BSI) according to the guidelines for animal experimentation and introduced at NIG. The TCA-GFP Tg construct was created by modifying the RP23-39F11 BAC clone derived from C57Bl/6 (B6) mouse genomic DNA. The BAC construct was microinjected into B6 fertilized eggs to generate TCA-GFP mice. Only TCA-GFP;$NR1^{f/+}$ males (with a pure B6 background) and $NR1^{f/f}$ females (backcrossed from B6 to ICR more than three times) were used to produce TCA-GFP;$NR1^{f/+}$ and TCA-GFP;$NR1^{f/f}$ samples.

Supernova System

For the SnRFP experiments, a solution containing pTRE-Cre (10 ng/μl) and pCAG-loxP-STOP-loxP-RFP-ires-tTA-WPRE (1 μg/μl) was used. For the SnGCaMP3 experiments, a solution containing pTRE-Cre (10 ng/μl) and pCAG-loxP-STOP-loxP-GCaMP3-ires-tTA-WPRE (1 μg/μl) was used.

Electrophysiology

Coronal slices of barrel cortex (400 μm thick) were prepared from P5–P7 mice and EPSCs were recorded from SnRFP-positive neurons in L4. Spontaneous and miniature EPSCs were recorded at −70 mV, which is the reversal potential of inhibitory postsynaptic currents (IPSCs). The latter was recorded in the presence of 1 μM tetrodotoxin to block Na^+ channels. For analysis of AMPA/NMDA ratio, EPSCs were evoked by electrical stimulation of the white matter. AMPA receptor-mediated EPSCs were recorded at −70 mV in the presence of 10 μM SR95531 to block $GABA_A$ receptors. NMDA receptor-mediated EPSCs were recorded at +40 mV in the presence of 10 μM SR95531 and 10 μM NBQX, non-NMDA receptor antagonist. Electrophysiological experiments were performed according to the guidelines for animal experimentation of the National Institute for Physiological Sciences (NIPS).

Histology and Confocal Microscopy

Mice were overdosed with an intraperitoneal injection of pentobarbital, and coronal and tangential brain sections (50 or 100 μm) were obtained. Morphologies of the RFP-labeled barrel cells and GFP-labeled TC axons were observed using a TCS SP5 confocal microscope (Leica). For dendritic spine analysis, the second segments of the inner dendrites were imaged using a 63× objective lens (1.3 NA). The spine density was calculated in 20 μm segments.

Two-Photon Microscopy

For in vivo time-lapse imaging of the neonatal (P4 and P5) mouse barrel cortex, a small cranial window (500 μm in diameter) was made, and a customized titanium bar (approximately 30 mg) was attached to the adjacent cranial area. No apparent surgery-induced discomfort was observed. These pups drank milk as usual, and their behavior was indistinguishable from untreated littermates (Movie S2). Mice were anesthetized with 0.7%–0.9% isoflurane during imaging. In vivo images were acquired using an LSM 7MP multiphoton microscope (Zeiss) with a Mai Tai eHP DeepSee titanium-sapphire laser (Spectra-Physics) running at 1,000 nm, a BiG detector, and a 20× objective lens (1.05 NA). Between the imaging sessions, the pups were placed in a small cage on a 37°C heater with their littermates and provided warmed milk and gentle whisker stimulation with a soft brush every 2–3 hr (see Figure S3A). All pups appeared healthy after the last imaging session.

Image Analysis, Quantification, and Statistics

Acquired three-dimensional images from histology and in vivo imaging were analyzed using the IMARIS Filament Tracer software (Bitplane). Barrel cells (L4 spiny stellate neurons) and star pyramidal cells were distinguished by the absence and presence of an apical dendrite, respectively, and only barrel cells that adapted to the following criteria were used for the quantitative analysis: (1) those that were labeled with RFP at high intensity (RFP^{high}; neurons showing clear dendritic morphologies), (2) those that belonged to large barrels (arcs 1–5), and (3) those that were located at the edge of the GFP-labeled TC axon clusters.

Data analyses were conducted under strict genotype-blind conditions, and the genotypes were disclosed to the experimenter only after all experiments and analyses (dendrite tracing, dendritic length measurement, dendritic tip counting, and spine counting) were completed.

Statistical analyses were performed using Microsoft Excel, SPSS Statistics Base, and R version 3.0.1 (The R Foundation for Statistical Computing). To determine the appropriate statistical method, we analyzed normal distribution of the data using the one-sample Kolmogorov-Smirnov test. Significance of the differences was assessed by a two-tailed unpaired t test unless otherwise noted. Values are given as means ± SE. The asterisks in the figures indicate the following: $^*p < 0.05$, $^{**}p < 0.01$, and $^{***}p < 0.001$.

SUPPLEMENTAL INFORMATION

Supplemental Information includes Supplemental Experimental Procedures, four figures, one table, and four movies and can be found with this article online at http://dx.doi.org/10.1016/j.neuron.2014.02.026.

ACKNOWLEDGMENTS

We thank H. Nishiyama, H. Hirase, K. Kitamura, M. Matsuzaki, H. Miyawaki, and K. Sohya for advice on two-photon microscope imaging; H. Tanaka for advice on neuronal culture; T. Hirano and Y. Ikegaya for advice on in vitro calcium imaging; M. Kanbayashi and S. Kouyama for technical assistance; RIKEN BSI Research Resource Center for microinjection; S. Kawaguchi, J. Miyazaki, and S. Tonegawa for the pCAGplay vector, the CAG promoter, and the NR1 floxed mice, respectively; J. Miyazaki and Y. Saga for the CAG-CAT-EGFP Tg mice; Y. Bando and Y. Tagawa for the CAG-Syn-GFP vector; Y. Tagawa, H. Nishiyama, and Iwasato lab members for comments on the manuscript; R. Iwata and other Iwasato lab members for valuable discussion. This work was supported by JSPS KAKENHI (22700347 and 25640015) to H.M.; FIRST program to S.I.; and MEXT KAKENHI (22115009 and 21115519), the Naito Foundation, the Mitsubishi Foundation, Yamada Science Foundation, and the Uehara Memorial Foundation to T.I. W.L. was supported by the JSPS and the Iwatani Naoji Foundation.

Accepted: February 5, 2014
Published: March 27, 2014

REFERENCES

Ballester-Rosado, C.J., Albright, M.J., Wu, C.S., Liao, C.C., Zhu, J., Xu, J., Lee, L.J., and Lu, H.C. (2010). mGluR5 in cortical excitatory neurons exerts both cell-autonomous and -nonautonomous influences on cortical somatosensory circuit formation. J. Neurosci. *30*, 16896–16909.

Barnett, M.W., Watson, R.F., and Kind, P.C. (2006a). Pathways to barrel development. In Development and Plasticity in Sensory Thalamus and Cortex, R. Erzurumlu, W. Guide, and Z. Molnar, eds. (New York: Springer), pp. 138–157.

Barnett, M.W., Watson, R.F., Vitalis, T., Porter, K., Komiyama, N.H., Stoney, P.N., Gillingwater, T.H., Grant, S.G., and Kind, P.C. (2006b). Synaptic Ras GTPase activating protein regulates pattern formation in the trigeminal system of mice. J. Neurosci. *26*, 1355–1365.

Boyden, E.S., Zhang, F., Bamberg, E., Nagel, G., and Deisseroth, K. (2005). Millisecond-timescale, genetically targeted optical control of neural activity. Nat. Neurosci. *8*, 1263–1268.

Bureau, I., von Saint Paul, F., and Svoboda, K. (2006). Interdigitated paralemniscal and lemniscal pathways in the mouse barrel cortex. PLoS Biol. *4*, e382.

Callaway, E.M., and Borrell, V. (2011). Developmental sculpting of dendritic morphology of layer 4 neurons in visual cortex: influence of retinal input. J. Neurosci. *31*, 7456–7470.

Carrillo, J., Nishiyama, N., and Nishiyama, H. (2013). Dendritic translocation establishes the winner in cerebellar climbing fiber synapse elimination. J. Neurosci. *33*, 7641–7653.

Cases, O., Vitalis, T., Seif, I., De Maeyer, E., Sotelo, C., and Gaspar, P. (1996). Lack of barrels in the somatosensory cortex of monoamine oxidase A-deficient mice: role of a serotonin excess during the critical period. Neuron *16*, 297–307.

Chen, T.W., Wardill, T.J., Sun, Y., Pulver, S.R., Renninger, S.L., Baohan, A., Schreiter, E.R., Kerr, R.A., Orger, M.B., Jayaraman, V., et al. (2013). Ultrasensitive fluorescent proteins for imaging neuronal activity. Nature *499*, 295–300.

Cline, H.T., and Constantine-Paton, M. (1990). NMDA receptor agonist and antagonists alter retinal ganglion cell arbor structure in the developing frog retinotectal projection. J. Neurosci. *10*, 1197–1216.

Crair, M.C., and Malenka, R.C. (1995). A critical period for long-term potentiation at thalamocortical synapses. Nature *375*, 325–328.

Datwani, A., Iwasato, T., Itohara, S., and Erzurumlu, R.S. (2002). NMDA receptor-dependent pattern transfer from afferents to postsynaptic cells and dendritic differentiation in the barrel cortex. Mol. Cell. Neurosci. *21*, 477–492.

Dhande, O.S., Hua, E.W., Guh, E., Yeh, J., Bhatt, S., Zhang, Y., Ruthazer, E.S., Feller, M.B., and Crair, M.C. (2011). Development of single retinofugal axon arbors in normal and β2 knock-out mice. J. Neurosci. *31*, 3384–3399.

Erzurumlu, R.S., and Jhaveri, S. (1990). Thalamic axons confer a blueprint of the sensory periphery onto the developing rat somatosensory cortex. Brain Res. Dev. Brain Res. *56*, 229–234.

Erzurumlu, R.S., and Kind, P.C. (2001). Neural activity: sculptor of 'barrels' in the neocortex. Trends Neurosci. *24*, 589–595.

Espinosa, J.S., Wheeler, D.G., Tsien, R.W., and Luo, L. (2009). Uncoupling dendrite growth and patterning: single-cell knockout analysis of NMDA receptor 2B. Neuron *62*, 205–217.

Fox, K. (2008). Barrel Cortex. (Cambridge: Cambridge University Press).

Goodman, C.S., and Shatz, C.J. (1993). Developmental mechanisms that generate precise patterns of neuronal connectivity. Cell Suppl. *72*, 77–98.

Greenough, W.T., and Chang, F.L. (1988). Dendritic pattern formation involves both oriented regression and oriented growth in the barrels of mouse somatosensory cortex. Brain Res. *471*, 148–152.

Hannan, A.J., Blakemore, C., Katsnelson, A., Vitalis, T., Huber, K.M., Bear, M., Roder, J., Kim, D., Shin, H.S., and Kind, P.C. (2001). PLC-beta1, activated via mGluRs, mediates activity-dependent differentiation in cerebral cortex. Nat. Neurosci. *4*, 282–288.

Hubel, D.H., Wiesel, T.N., and LeVay, S. (1977). Plasticity of ocular dominance columns in monkey striate cortex. Philos. Trans. R. Soc. Lond. B Biol. Sci. *278*, 377–409.

Inan, M., and Crair, M.C. (2007). Development of cortical maps: perspectives from the barrel cortex. Neuroscientist *13*, 49–61.

Ince-Dunn, G., Hall, B.J., Hu, S.C., Ripley, B., Huganir, R.L., Olson, J.M., Tapscott, S.J., and Ghosh, A. (2006). Regulation of thalamocortical patterning and synaptic maturation by NeuroD2. Neuron *49*, 683–695.

Iwasato, T., Erzurumlu, R.S., Huerta, P.T., Chen, D.F., Sasaoka, T., Ulupinar, E., and Tonegawa, S. (1997). NMDA receptor-dependent refinement of somatotopic maps. Neuron *19*, 1201–1210.

Iwasato, T., Datwani, A., Wolf, A.M., Nishiyama, H., Taguchi, Y., Tonegawa, S., Knöpfel, T., Erzurumlu, R.S., and Itohara, S. (2000). Cortex-restricted disruption of NMDAR1 impairs neuronal patterns in the barrel cortex. Nature *406*, 726–731.

Iwasato, T., Katoh, H., Nishimaru, H., Ishikawa, Y., Inoue, H., Saito, Y.M., Ando, R., Iwama, M., Takahashi, R., Negishi, M., and Itohara, S. (2007). Rac-GAP alpha-chimerin regulates motor-circuit formation as a key mediator of EphrinB3/EphA4 forward signaling. Cell *130*, 742–753.

Iwasato, T., Inan, M., Kanki, H., Erzurumlu, R.S., Itohara, S., and Crair, M.C. (2008). Cortical adenylyl cyclase 1 is required for thalamocortical synapse maturation and aspects of layer IV barrel development. J. Neurosci. *28*, 5931–5943.

Katz, L.C., and Shatz, C.J. (1996). Synaptic activity and the construction of cortical circuits. Science *274*, 1133–1138.

Konur, S., and Ghosh, A. (2005). Calcium signaling and the control of dendritic development. Neuron *46*, 401–405.

Lee, L.J., Iwasato, T., Itohara, S., and Erzurumlu, R.S. (2005). Exuberant thalamocortical axon arborization in cortex-specific NMDAR1 knockout mice. J. Comp. Neurol. *485*, 280–292.

Lefort, S., Tomm, C., Floyd Sarria, J.C., and Petersen, C.C. (2009). The excitatory neuronal network of the C2 barrel column in mouse primary somatosensory cortex. Neuron *61*, 301–316.

Li, Y., Lu, H., Cheng, P.L., Ge, S., Xu, H., Shi, S.H., and Dan, Y. (2012). Clonally related visual cortical neurons show similar stimulus feature selectivity. Nature *486*, 118–121.

Li, H., Fertuzinhos, S., Mohns, E., Hnasko, T.S., Verhage, M., Edwards, R., Sestan, N., and Crair, M.C. (2013). Laminar and columnar development of barrel cortex relies on thalamocortical neurotransmission. Neuron *79*, 970–986.

Matsui, A., Tran, M., Yoshida, A.C., Kikuchi, S.S., U, M., Ogawa, M., and Shimogori, T. (2013). BTBD3 controls dendrite orientation toward active axons in mammalian neocortex. Science *342*, 1114–1118.

Mizuno, H., Hirano, T., and Tagawa, Y. (2007). Evidence for activity-dependent cortical wiring: formation of interhemispheric connections in neonatal mouse visual cortex requires projection neuron activity. J. Neurosci. *27*, 6760–6770.

Nakai, J., Ohkura, M., and Imoto, K. (2001). A high signal-to-noise Ca(2+) probe composed of a single green fluorescent protein. Nat. Biotechnol. *19*, 137–141.

Narboux-Nême, N., Evrard, A., Ferezou, I., Erzurumlu, R.S., Kaeser, P.S., Lainé, J., Rossier, J., Ropert, N., Südhof, T.C., and Gaspar, P. (2012). Neurotransmitter release at the thalamocortical synapse instructs barrel formation but not axon patterning in the somatosensory cortex. J. Neurosci. *32*, 6183–6196.

Niell, C.M., Meyer, M.P., and Smith, S.J. (2004). In vivo imaging of synapse formation on a growing dendritic arbor. Nat. Neurosci. *7*, 254–260.

Ohsaki, K., Osumi, N., and Nakamura, S. (2002). Altered whisker patterns induced by ectopic expression of Shh are topographically represented by barrels. Brain Res. Dev. Brain Res. *137*, 159–170.

Persico, A.M., Mengual, E., Moessner, R., Hall, F.S., Revay, R.S., Sora, I., Arellano, J., DeFelipe, J., Gimenez-Amaya, J.M., Conciatori, M., et al. (2001). Barrel pattern formation requires serotonin uptake by thalamocortical afferents, and not vesicular monoamine release. J. Neurosci. *21*, 6862–6873.

Petersen, C.C. (2007). The functional organization of the barrel cortex. Neuron *56*, 339–355.

Saito, T., and Nakatsuji, N. (2001). Efficient gene transfer into the embryonic mouse brain using in vivo electroporation. Dev. Biol. *240*, 237–246.

Saneyoshi, T., Wayman, G., Fortin, D., Davare, M., Hoshi, N., Nozaki, N., Natsume, T., and Soderling, T.R. (2008). Activity-dependent synaptogenesis: regulation by a CaM-kinase kinase/CaM-kinase I/betaPIX signaling complex. Neuron *57*, 94–107.

Sato, H., Fukutani, Y., Yamamoto, Y., Tatara, E., Takemoto, M., Shimamura, K., and Yamamoto, N. (2012). Thalamus-derived molecules promote survival and dendritic growth of developing cortical neurons. J. Neurosci. *32*, 15388–15402.

Sin, W.C., Haas, K., Ruthazer, E.S., and Cline, H.T. (2002). Dendrite growth increased by visual activity requires NMDA receptor and Rho GTPases. Nature *419*, 475–480.

Staiger, J.F., Flagmeyer, I., Schubert, D., Zilles, K., Kötter, R., and Luhmann, H.J. (2004). Functional diversity of layer IV spiny neurons in rat somatosensory cortex: quantitative morphology of electrophysiologically characterized and biocytin labeled cells. Cereb. Cortex *14*, 690–701.

Sur, M., and Rubenstein, J.L. (2005). Patterning and plasticity of the cerebral cortex. Science *310*, 805–810.

Svoboda, K., Denk, W., Kleinfeld, D., and Tank, D.W. (1997). In vivo dendritic calcium dynamics in neocortical pyramidal neurons. Nature *385*, 161–165.

Tabata, H., and Nakajima, K. (2001). Efficient in utero gene transfer system to the developing mouse brain using electroporation: visualization of neuronal migration in the developing cortex. Neuroscience *103*, 865–872.

Tsien, J.Z., Huerta, P.T., and Tonegawa, S. (1996). The essential role of hippocampal CA1 NMDA receptor-dependent synaptic plasticity in spatial memory. Cell *87*, 1327–1338.

Van de Ven, T.J., VanDongen, H.M., and VanDongen, A.M. (2005). The nonkinase phorbol ester receptor alpha 1-chimerin binds the NMDA receptor NR2A subunit and regulates dendritic spine density. J. Neurosci. *25*, 9488–9496.

Welker, E., Armstrong-James, M., Bronchti, G., Ourednik, W., Gheorghita-Baechler, F., Dubois, R., Guernsey, D.L., Van der Loos, H., and Neumann, P.E. (1996). Altered sensory processing in the somatosensory cortex of the mouse mutant barrelless. Science *271*, 1864–1867.

Wong, R.O., and Ghosh, A. (2002). Activity-dependent regulation of dendritic growth and patterning. Nat. Rev. Neurosci. *3*, 803–812.

Woolsey, T.A., and Van der Loos, H. (1970). The structural organization of layer IV in the somatosensory region (SI) of mouse cerebral cortex. The description of a cortical field composed of discrete cytoarchitectonic units. Brain Res. *17*, 205–242.

Woolsey, T.A., and Wann, J.R. (1976). Areal changes in mouse cortical barrels following vibrissal damage at different postnatal ages. J. Comp. Neurol. *170*, 53–66.

Woolsey, T.A., Dierker, M.L., and Wann, D.F. (1975). Mouse SmI cortex: qualitative and quantitative classification of golgi-impregnated barrel neurons. Proc. Natl. Acad. Sci. USA *72*, 2165–2169.

Wu, C.S., Ballester Rosado, C.J., and Lu, H.C. (2011). What can we get from 'barrels': the rodent barrel cortex as a model for studying the establishment of neural circuits. Eur. J. Neurosci. *34*, 1663–1676.

Xie, Z., Srivastava, D.P., Photowala, H., Kai, L., Cahill, M.E., Woolfrey, K.M., Shum, C.Y., Surmeier, D.J., and Penzes, P. (2007). Kalirin-7 controls activity-dependent structural and functional plasticity of dendritic spines. Neuron *56*, 640–656.

Young, P., Qiu, L., Wang, D., Zhao, S., Gross, J., and Feng, G. (2008). Single-neuron labeling with inducible Cre-mediated knockout in transgenic mice. Nat. Neurosci. *11*, 721–728.

Zong, H., Espinosa, J.S., Su, H.H., Muzumdar, M.D., and Luo, L. (2005). Mosaic analysis with double markers in mice. Cell *121*, 479–492.